LAWRENCE
LIVERMORE
NATIONAL
LABORATORY

LLNL-TR-864495

Fluoropolymer Aging Phenomena

C. Orme, X. Xu, M. Marple, J. Lewicki

May 16, 2024

Disclaimer

This work performed under the auspices of the U.S. Department of Energy by Lawrence Livermore National Laboratory under Contract DE-AC52-07NA27344.

Fluoropolymer Aging Phenomena

C. A. Orme, M. Marple, X. Xu, and J. Lewicki

1 Introduction

This project aims to investigate structural and morphological changes in fluoropolymers induced by both processing and aging phenomena such as heat, time, and irradiation. Fluoropolymers are an important class of thermoplastics that are broadly used in industry as o-rings and seals when chemical resistance and thermal performance are important. They are also often used in thin film geometries as binders in batteries, insulation layers, water barriers, and anti-fouling coatings. For all of these applications, mechanical integrity and aging are important aspects of their use. Changes in the crystalline morphology are known to impact the mechanical properties of the polymer and can lead to failure. The broad goals of this project are to correlate compositional changes, morphological changes, and mechanical changes. report focuses on the morphological changes that are correlated with nuclear magnetic resonance (NMR), calorimetry and mechanical testing. We plan to compare structure and morphology measurements across complementary bulk and surface techniques. We use in situ atomic force microscopy (AFM) to measure domain shape and crystallization kinetics; in situ NMR to measure crystalline composition; and differential scanning calorimetry (DSC) to measure melting temperatures.

2 Crystallization signatures of CTFE-co-VDF fluoropolymers

In this study we used hot-stage atomic force microscopy, NMR and DSC to study fluoropolymer crystallization kinetics with an emphasis on fluoropolymer binder FK-800 and Kel-F, which are random copolymers composed nominally of 75±4% chlorotrifluorethylene (CTFE) and 25 ± 4% vinylidene fluoride (VDF). In this report we have broken our results into two section: (1) *Progress on Lot-Time-Temperature Characterization, which details our work towards developing a database*; (2) *^{19}F Solid-State NMR Spectroscopy and Relaxometry on FK-800 and Kel-F 800*; and (3) *Multi-modal characterization*.

2.1 Progress on Lot-Time-Temperature Characterization

In previous work, our (*ex situ*) studies on CTFE-VDF thin films revealed unexpected crystallization patterns. We expected that increasing the CTFE content from 73 to 79% would lead to faster crystal growth and more nucleation sites. However, we found that both the growth rates and the nucleation density varied widely without a clear trend with CTFE composition. These results suggest that there are other factors, beyond CTFE content, that significantly affect crystallization in these films. For example, an impurity that either promotes or hinders crystal formation. Without knowledge of this variable the system is not fully specified and we don't expect to be able to predict lot-to-lot variations. For this reason we have adopted a database approach to measure the kinetic parameters and sought a means to connect fundamental measures (nucleation density and growth rate) with more performance-related parameters such as percent crystallinity.

To this end, we looked deeper into one specific film composition using *in situ* temperature-dependent crystallization studies. Employing the Avrami equation, customized with rates and exponents extracted

from measured data, we successfully modeled the time evolution of crystallinity for ten temperatures. We then tested the use of the Avrami equation across 9 lots and with a few exceptions, found good fits. In particular for lots we found:

- Kel-F lots showed a high degree of variability in growth and nucleation – two orders of magnitude - similar to that found for the earlier composition studies on FK-800 formulations.
- Nucleation density and growth rate lacked expected correlation, suggesting factors beyond CTFE content (and supersaturation) influence kinetics. This is consistent with our early composition study that also showed that kinetics did not trend simply with CTFE content.
- Most crystallinity versus time data for films aged at 50°C is well-described by approximating the system as instantaneous nucleation (leading to Avrami exponents of n=1 or n=2) and calculating an Avrami rate constant based on the nucleation density and radial growth rate.

In this study, we continue this approach with a focus on 12 FK-800 formulations.

2.1.1 Lot-to-lot variation in crystallization kinetics

This study categorized lot variations through visual inspection of film morphology after 48 hours of thermal aging at 50°C, aiming to identify groups with similar aging behavior (Figure 1). As depicted by the columns in Figure 1, four initial groupings emerged based on combinations of high/low nucleation density (ND) and high/low growth rate (GR). Additionally, we identified a fifth distinct category with "fiber and other morphologies"

Each category exhibits distinct characteristics:

- Low ND & Low GR (blue): Sparse growth, taking months to fully crystallize with few isolated crystals embedded in amorphous polymer.
- High ND & Low GR (yellow): Numerous nuclei but slow crystal growth, possibly due to a high concentration of impurities or surfactants pinning step edges.
- Low ND & High GR (green): Rapid crystal growth with additional nucleation occurring on top of existing crystals (second layer) instead of primarily from the amorphous layer.
- High ND & High GR (red): Fully crystalline within a day or two at 50°C due to high nucleation and growth rates.
- Fiber and other: Non-disk-like growth or unusual nucleation behavior, often featuring a fiber growth morphology with crystals growing perpendicular to the substrate. This category was not quantitatively evaluated because it requires adjustments to our current measurement protocols for proper kinetic analysis.

Of the 28 visualized lots, roughly a third (10 out of 28) belong to the slow-growing, blue category, with the remaining categories receiving relatively even distribution with 4-5 lots each.

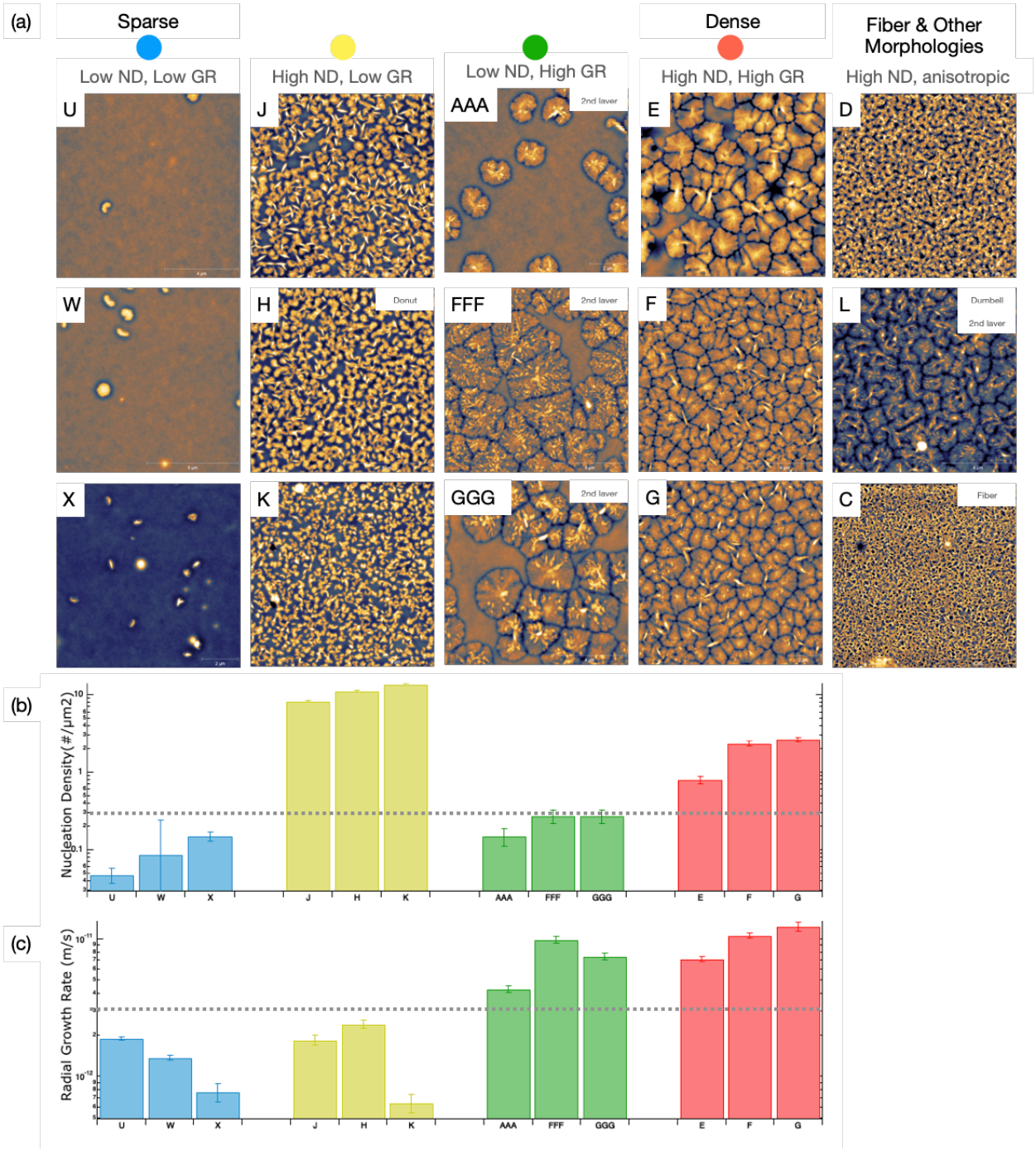

Figure 1. Crystallization behavior of twelve lots of FK-800 categorized by nucleation density (ND) and initial linear radial growth rate (GR) for predominately disk-like morphologies. (a) AFM images of FK-800 thin films after thermal aging for 48 hours at 50°C. All images are 10µm x10µm and have a z-scale of 20 nm. The first four columns show examples with high and low ND and high and low GR. The last columns shows examples of non-disk-like growth which can not be analyzed in the same way. (b) Steady-state nucleation density and (c) radial growth rate are shown on a log scale below the images. The horizontal dashed line provides an approximate delination between "high" and "low" with low nucleation density below ~ 0.3 crystals per μm^2 and low growth rate below ~$3x10^{-12}$ m/s.

While this initial classification relied on visual inspection, it has been improved by quantifying crystallization parameters. The nucleation density was measured as a function of time and the *steady-state nucleation density* was obtained from this curve once the nucleation rate drops close to zero, but before the crystals have merged. The steady state nucleation density ranges from 0.05 to 13 μm^{-2}, and is plotted on a log plot to highlight the two-orders of magnitude variation (Figure 1b). The *early-time radial growth rate* was measured from a sequence of images using isolated crystals. The average radial growth rate ranges from 6 x 10^{-13} to 1 x 10^{-11} m/s, and is plotted on a log plot to highlight the order of magnitude variation (Figure 1c). This allows us to define "high nucleation" as exceeding ~0.3 crystals/μm^2 and "high growth rate" exceeding ~3x10^{-12} m/s, as indicated by the dashed grey lines.

To further quantify the kinetics of of the twelve lots, we measured the **fraction of the surface covered with crystals** as a function of time from trajectories exemplified by those in Figure 2.

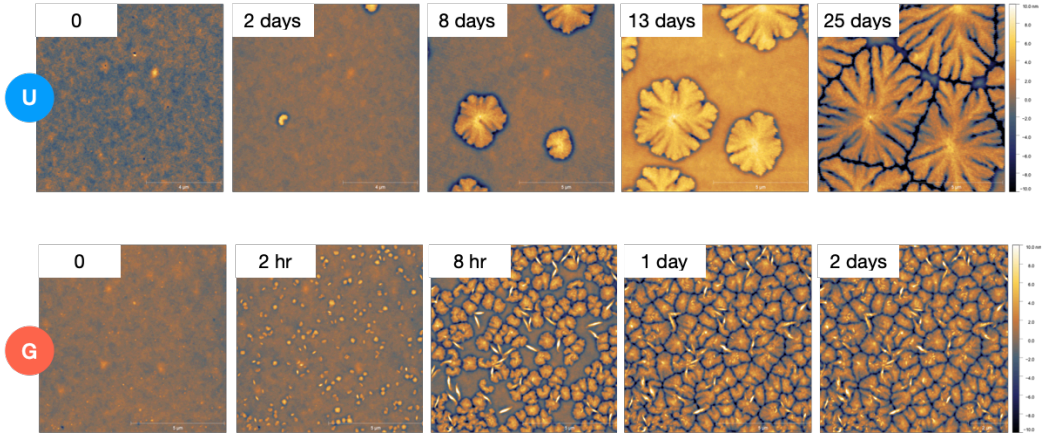

Figure 2. Trajectories for two lots measured using hot-stage AFM. All images are 10µm x10µm and have a z-scale of 20 nm as indicated by false color scale at the right. The top row shows an example of a low ND, low GR (blue) category over 25 days and the bottom row shows an example of a high ND, high GR (red) category over 2 days.

The fraction of the surface crystallized rises slowly at first, accelerates, and then levels off. The traditional S-shaped curve is often modeled using the Avrami equation,

$$f_c(\mathrm{t}) = 1 - e^{-k_a t^n} \qquad (1)$$

where, for our two-dimensional films, $f_c(t)$ is the areal fraction of the surface that has crystallized, k_a is the *Avrami rate constant*, t is time and n is the *Avrami exponent* which can vary typically between 1 and 3 for 2D growth. The Avrami rate constant and exponent can either be fitted from crystallization curves or they can be calculated for specific cases that depend upon the mode of nucleation, the form of the growth rate and the dimensionality of the growth. We take both approaches and compare them. The relationship between measurable crystal growth parameters and the Avrami exponent and rate constant are depicted in Figure 3. For “instantaneous nucleation” the Avrami exponents are 1 or 2 and depend on the nucleation density (***ρ***) and the radial growth rate whereas for continual or “progressive” nucleation the avrami exponents are 2 or 3 and depend on the nucleation rate (ν’) and the radial growth rates.

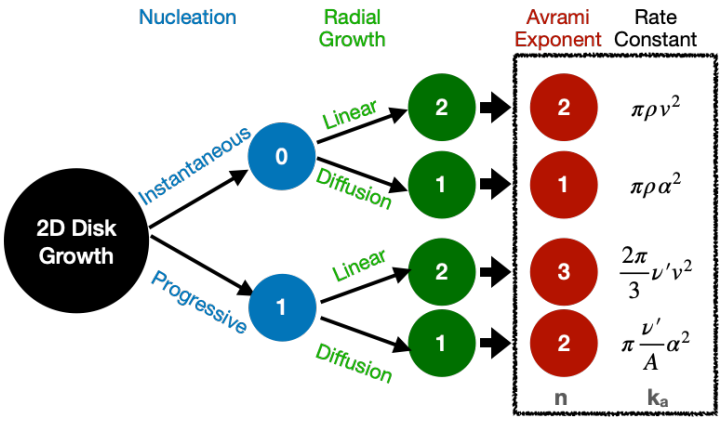

Figure 3. Relationship between crystal growth parameters and Avrami exponents (n) and rate constants (k_a) for disk-like 2D growth. The Avrami exponent (red) is the sum of contributions from nucleation (blue) and growth (green). The rate constants depend on nucleation nucleation density (***ρ***) or nucleation rate (ν') depending on whether nucleation is instantaneous or progressive, respectively. k_a also depends on whether the radius (r) grows linearly with time ($r = vt$) or as the square root of time ($r = \alpha t^{0.5}$).

Figure 4 summarizes our Avrami analysis of crystallization verus time. Figure 4a plots the 12 lots together to show the significant disparities in crystallization completion times across the different lot categories. The slow-growing blue category requires over 25 days, while the fastest growing red category achieves full crystallization within approximately 2 days. Notably, the **yellow lot data exhibits an atypical slowdown** before reaching completion.This observation may indicate the presence of impurities that segregate to crystal step edges, hindering their growth.

To further analyze the crystallization kinetics, Avrami curve fits were applied to each category (Figures 4b-e). Initial unconstrained fits (Table, Figure 4f) yielded a range of rate constants with fractional n values, varying from 0.7 to 2.7. However, varying n values resulted in incompatible rate constant units, preventing their direct comparison. Instead we refit the curves, choosing n=2 when the unconstrained fit had values of 1.6-2.7 and n=1 when the unconstrained fit had values of 0.7-1.6. These constraints resulted in n=2 for low nucleation density lots (blue and green) and n=1 for high nucleation density lots (yellow and red). An Avrami exponent of 1 suggests **diffusion-limited radial growth for the high nucleation density lots (yellow and red)** (Figure 3); this is very reasonable because we expect greater competition for material when the nearest neighbor spacings are smaller.

To **calculate rate constants**, we assumed **instantaneous nucleation** for all lots based on the observation that 80% of the nucleation events happened before the surface reached a fractional coverage of just 4%. This suggests that the observed phase change curve in Figure 4a primarily reflects crystal growth dynamics, with minimal influence from ongoing nucleation. To further support this assumption, Figure 4b-d uses bars to show the times required for each lot to reach 80% of their steady-state nucleation density. This finding is consistent with our FY22 report, which showed that homogeneous nucleation only dominates at high driving forces close to the glass transition temperature (28°C) and concluded that heterogeneous nucleation is the primary driver of nucleation density at 50°C. For instantaneous nucleation, the rate constants (Figure 3) depend on the nucleation density (***ρ*** , values in Figure 1b) and the radial growth rate with the radius (r) changing linearly with time (r=vt, values in Figure 1c) or as the square root of time ($r=\alpha t^{0.5}$, values not shown). The calculated values are tabulated in the Figure 4f and compared with measured rate constants in Figure 4g. The fitted and calculated values all agree within a factor of ~2.

The fitted and calculated rate constants demonstrate satisfactory agreement for the majority of lots, with a maximum discrepancy observed for lot H, where they differ by a factor of 2.3. Considering the independent nature of nucleation density, growth rate, and fractional coverage measurements, this level of agreement is encouraging. Also, it should be noted that the calculated Avrami constants displayed in Figure 3 are based on the assumption of time-invariant rates. Consequently, effects such as crystal growth pinning or transitions from linear to diffusion-limited growth cannot be accurately captured by this simplified model. For example, we do not expect the yellow lots to be accurately captured without including time-variant growth rates.
We also note that the original four groupings based on nucleation density and growth rate remain in tact by considering avrami exponent and threshold rate constants (dashed lines, Figure 4g).

Summary of finding for lot variations of FK-800:

- The (linear) growth rate at 50 °C for the twelve lots ranges between 8 x 10^{-13} and 1 x10^{-11} m/s, more than an order of magnitude.
- The nucleation density at 50 °C for the twelve lots ranges between 0.05 and 13.5 μm^{-2} , more than 2 orders of magnitude.
- Lots can be categorized based on whether their nucleation density is greater than or less than 3 crystals per square micron, and whether their growth rate is slower than or faster than 3 x10^{-12} m/s. Alternatively, these groupings can be obtained from the Avrami exponent and rate constants.
- Crystalline coverage verus time plots can be successfully fit using the Avrami Equation with n=1 or n=2, which corresponds to instantaneous nucleation, disk-like growth and radii that grow either as t^1 or t^0.5.

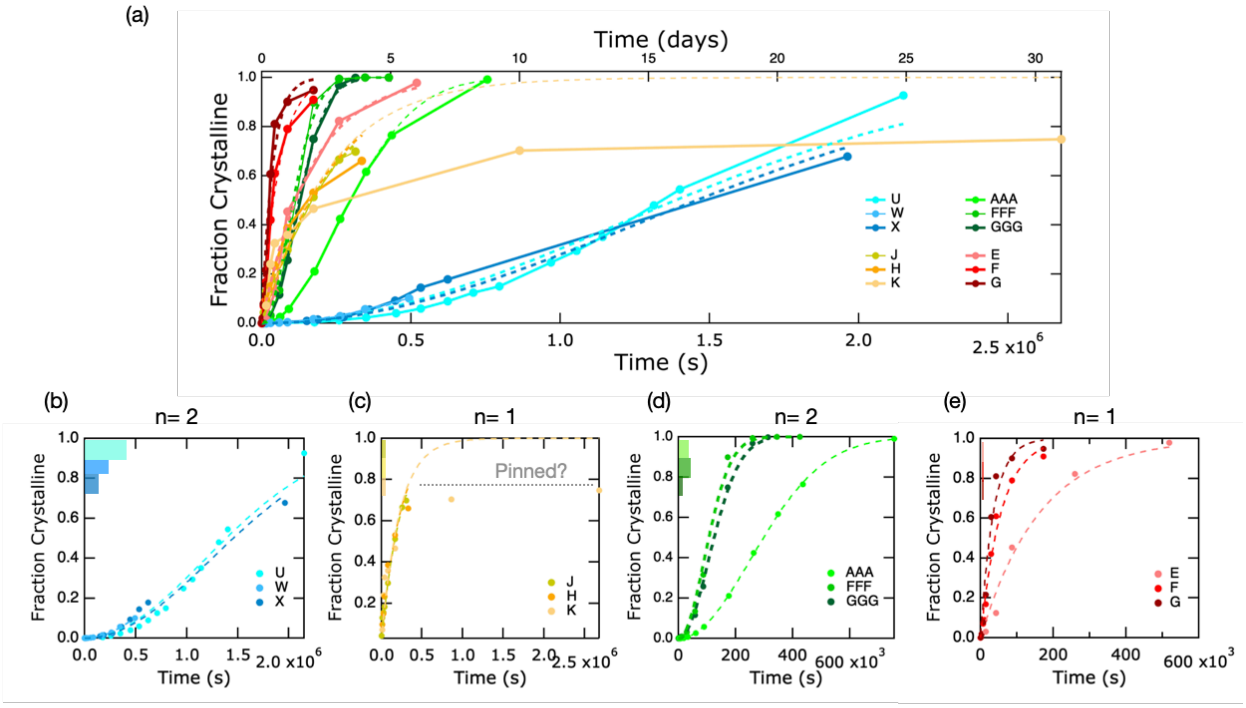

(f)

	Fit k_a & n		Fit k_a, constrain n		Calculate k_a
Lot	n	k_a	n	k_a	k_a
U	2.7	1.2E-17	2	3.6E-13	5.3E-13
W	1.9	2.8E-12	2	4.49E-13	5.1E-13
X	1.6	6.7E-11	2	3.27E-13	2.8E-13
J	0.9	2.3E-05	1	4.2E-06	7.6E-06
H	0.7	1.2E-04	1	4.3E-06	1.0E-05
K	0.6	5.3E-04	1	4.4E-06	6.4E-06
AAA	2.0	8.3E-12	2	7.8E-12	8.8E-12
FFF	2.5	1.1E-13	2	6.1E-11	8.2E-11
GGG	2.2	4.3E-12	2	4.4E-11	4.7E-11
E	1.2	4.0E-07	1	6.1E-06	4.9E-06
F	1.2	3.0E-06	1	1.8E-05	3.7E-05
G	1.6	4.1E-08	1	2.8E-05	3.2E-05

(g)

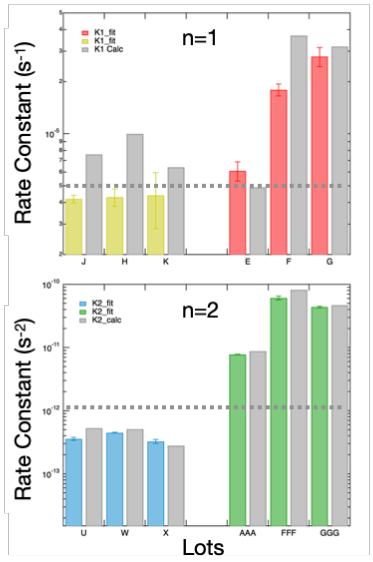

Figure 4. Crystallization behavior of twelve lots of FK-800 at 50°C. (a) Areal fraction of the film transformed to crystals. (b-e) Fraction crystalline versus time broken out by the 4 categories described in Figure 1. Data are shown as solid dots, color-coded according to lot. Dashed lines are Avrami fits with n=2 for (b) and (d) and n=1 for (c) and (e). Bars in the upper left corner of each graph indicate the time needed to achieve 80% of the steady-state nucleation density. Only lot U is arguably progressive nucleation; the others are consistent with instantaneous nucleation. (f) Table summarizing unconstrained and constrained Avrami fits to the crystallization data. The last column gives the calculated Avrami rate constant based on nucleation density ($\boldsymbol{\rho}$) and growth rates (v or α). (g) Comparison between measured and calculated rate constants for n=1 and n=2 using equations shown in Figure 3. Calculated values are shown in grey. Dashed lines indicate an approximate delination between "high" and "low" if Avrami exponent and Avrami rate constant were used to classify lots.

2.2 ^{19}F Solid-State NMR Spectroscopy and Relaxometry on FK-800 and Kel-F 800

Previous work (FY21-22) established 19F NMR relaxometry as a valuable tool for characterizing semicrystalline fluoropolymer polychlorotrifluoroethylene (PCTFE). We demonstrated its ability to (1) measure molecular motions, showing that amorphous regions relax faster due to higher mobility compared to rigid, crystalline domains, and (2) to estimate bulk crystallinity, with T1ρ rigid signal fractions accurately reflecting crystallinity (validated against DSC over the range of 30-65% crystalline). This finding suggests that $T_{1\rho}$ measurements could provide a relatively easy and non-destructive method for determining bulk crystallinity in fluoropolymers.

In FY23 we applied these techniques to FK-800 as a step towards developing a technique capable of characterizing and quantifying binder crystallinity within HE composites.
Towards this goal we have:

- Compared FK-800 with PCTFE
- Measured FK-800 as a function of temperature to identify the amorphous fingerprint.
- Compared spectral features of 6 Kel-F lots and 6 FK-800
- Estimated impurity size and concentration in the above 12 lots
- Worked towards developing quantitative methods to measure crystallization.

We have broken our results into sections: (1) *Spectral features of PCTFE, FK-800 and Kel-F* and (2) *Impurity attributes via spectral filtering of $T_{1\rho}$*.

2.2.1 Spectral Features of PCTFE, FK-800, and Kel-F

Comparing FK-800 and PCTFE: Solid-state NMR spectroscopy provides insights into the local chemical environments and allows us to distinguish between the VDF regions and CTFE regions. To illustrate the chemical environments, it is useful to compare the solid-state 19F NMR spectra of FK-800 to that of PCTFE (Figure 5). By comparing the 19F NMR spectra of FK-800 and PCTFE (Figure 5a), we can visualize these environments in detail. The PCTFE spectrum exhibits multiple broad peaks in two regions: -95 to -115 ppm and -123 to -137 ppm. These regions are assigned to fluorine atoms within -CF2- and -CClF- groups, respectively.Multiple peaks are observed for each F environment because of differences of stereochemical conformations of the monomer unit (-CF2-CFCl-), where various tetramer units with different combinations of head to head, head to tail, or tail to tail conformations can produce distinct peaks[2].The peaks are additionally broadened by structural disorder and further neighbor interactions. This demonstrates the sensitivity of the 19F to the structure of local chemical environments and poses a challenge when it comes to cleanly distinguishing between amorphous and crystalline phases, as both phases are considerably broadened. The introduction of a VDF monomer unit into PCTFE for FK-800 does not alter the spectra too much. Broadly the -CF2- and -CFCl- remain observable and have similar chemical shifts, however the VDF portion has a distinct peak between the -CF2- and -CFCl- regions.

Molecular dynamics and temperature, relative to the glass transition temperature (~31°C for FK-800, lot N) play an important role in obtaining peak resolution for polymeric materials. Below T_g, the polymer is a solid, with few molecular re-orientations of the chain structure, whereas above T_g, there are rapid motions of the chain. These rapid motions have an averaging effect on dipolar and chemical shift anisotropy interactions which cause the broadening observed in the ^{19}F spectra, thus spectra collected at high temperatures above T_g provide better insight into the ^{19}F chemical environments (Figure 5b).

Solid state ^{19}F spectra of FK-800 were collected from 0°C up to 120°C and shows progressive line narrowing. At the melting temperature (120°C), the spectra shows each of the three general regions contains at least three peaks; the individual peaks reflect the different stereochemical conformations. If needed, further identification of the stereochemical conformations can be elucidated by performing quantum chemical calculations on model clusters like the approach used for PCTFE[2]. In FY24 we plan to use the high resolution (120°C) data to identify the peak positions for multispectral decomposition analysis.

Summary of comparison between FK-800 vs PCTFE

- The three regions of interest are: -CF2- (-95 to -115 ppm) and -CFCl- (-123 to -137 ppm) from CTFE and the -CF2- from VDF (-115 to -125)
- Peak broadening poses challenge for distinguishing amorphous and crystalline regions
- Peak broadening is reduced above the melting point which clarifies the peak positions for spectral decomposition.

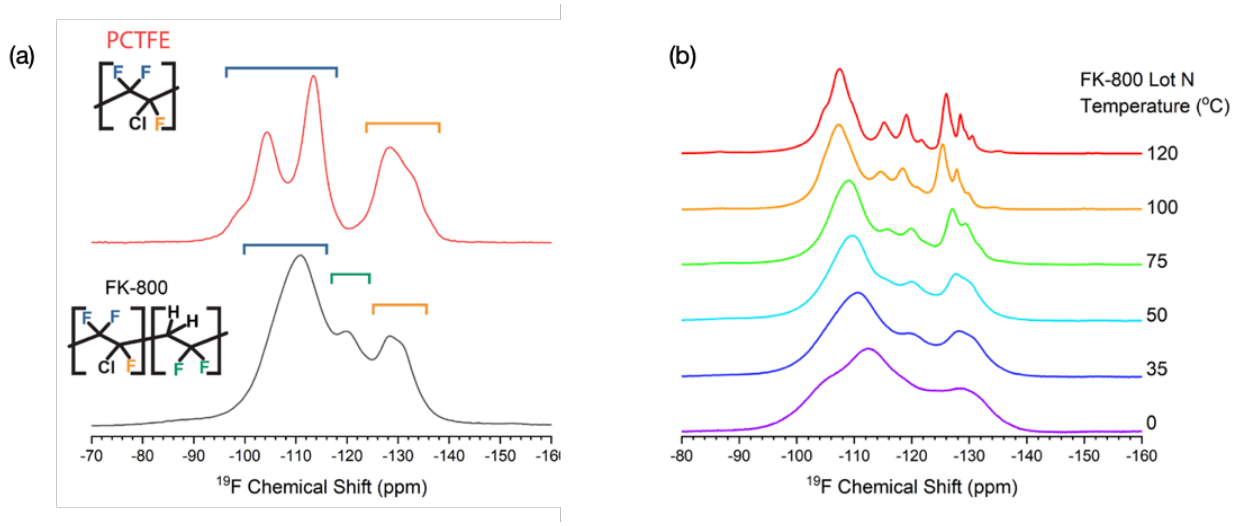

Figure 5 (a) Solid-state ^{19}F NMR spectra of PCTFE (top) and FK-800. Schematic of the monomers denote the chemical shift range for each fluorine environment, blue are for fluorine in -CF2-, orange for -CFCl-, and green for -CF2-CH2-. (b) Variable temperature solid-state ^{19}F spectra of FK-800, collected while spinning at 25 kHz.

Comparing FK-800 and Kel-F: To investigate potential chemical impacts on crystallization kinetics, several lots of FK-800 and Kel-F 800 were analyzed with 19F and 1H NMR. Figure 6 reveals consistent line shapes across all six FK-800 samples. This indicates identical chemical environments and suggests limited variation in PCTFE/PVDF stoichiometry (73.7-78.8% CTFE based on manufacturer data) within the detection range of our measurements. The exception is lot C which has an additional peak at -123 ppm, implying there is an impurity within the sample. The 1H spectra of the FK-800 lots (Figure 6b) are almost all identical, implying the VDF regions in the polymer are the same. The absence of an impurity peak in the 1H also indicates the impurity is a perfluorinated rather than a protonated fluorine compound. AFM images (Figure 6c) show that although the NMR spectral features are similar for these lots, the crystallization kinetics and morphologies can differ dramatically. Impurities may be one source of these differences.

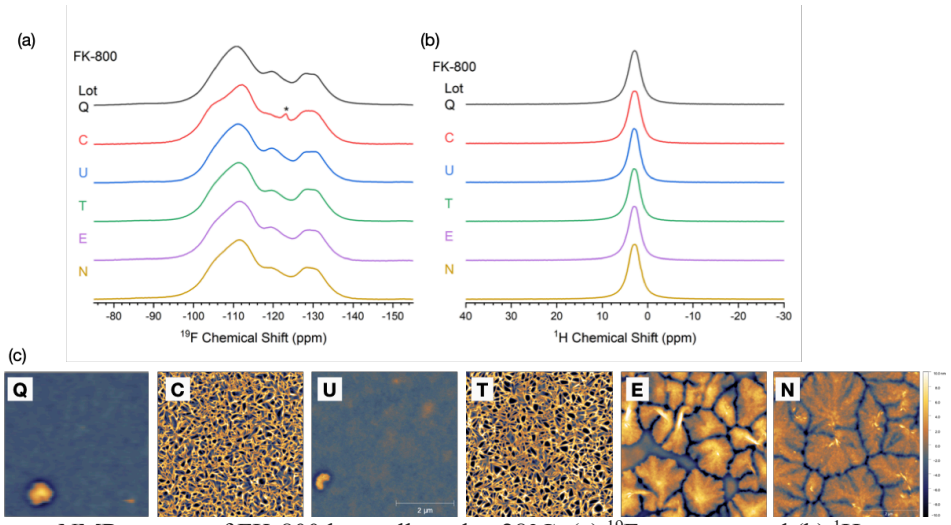

Figure 6 Solid-state NMR spectra of FK-800 lots collected at 28°C: (a) ^{19}F spectrum and (b) ^{1}H spectrum. Asterisks denote impurity peaks. (c) AFM of films aged for 48 hours at 50°C. Images are 5µmx5µm and 20nm z-scale .

Kel-F-800 spectra (Figure 7) resemble FK-800, but have more impurity peaks with distinct chemical shifts compared to FK-800 lot C. Kel-F was commonly synthesized with surfactants leading to two additional impurities at -83.6 ppm and -138.4 ppm. The ^{1}H spectra also show good agreement and given the lack of ^{1}H impurities in most of the lots, this suggests that these too are perfluorinated compounds. The exception is lot CC which has an impurity peak at 8 ppm. Deeper insight into the identity of these impurity peaks can be gained by future ^{19}F-^{13}C and ^{1}H-^{13}C NMR correlation measurements to isolate the ^{13}C chemical shifts associated with the impurity, aiding assignment. The common presence of impurities in the Kel-F lots may explain why they tend to have higher nucleation densities than present formulations.

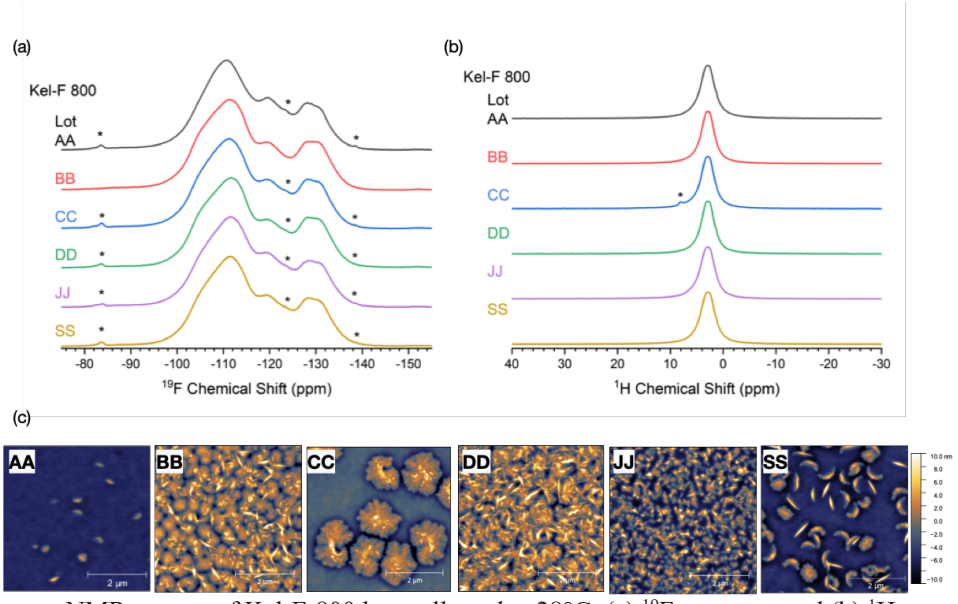

Figure 7 Solid-state NMR spectra of Kel-F-800 lots collected at 28°C: (a) ^{19}F spectrum and (b) ^{1}H spectrum. Asterisks are impurity peaks. (c) AFM of films aged for 48 hours at 50°C. Images are 5µmx5µm with 20nm z-scale.

2.2.2 Impurity attributes via spectral filtering of T1p

To investigate impurities, we used spin lattice relaxation in the rotating frame ($T_{1\rho}$) measurements as it is sensitive to molecular motions in the 10-100 kHz range. As demonstrated in previous years, $T_{1\rho}$ measurements can act as a relaxation based spectral filter for the rigid and mobile regions in the polymer. This occurs because the signal from the mobile regions rapidly decay during the spin lock duration leaving only the rigid regions in the spectra. A relaxation spectral filter addresses the issue of overlapping amorphous and crystalline peaks in ^{19}F NMR. Additionally, a $T_{1\rho}$ measurement provides relaxation times associated with the constituent phases which may provide insight into crystallization processes. To obtain both a filtered spectra of each phase and its associated $T_{1\rho}$ relaxation time, we use a multivariate curve resolution processing on the $T_{1\rho}$ dataset. The implementation we use is SCORE[3] (speedy component resolution), which fits a defined number of components to each spectra with an exponential decay function. The output of this processing provides a mobility based spectral filter showing the rigid and mobile components, their respective $T_{1\rho}$ relaxation times, as well as their contribution to the overall signal, thus providing insight into how much of the sample is 'rigid' at the given experimental conditions. For our previous demonstration on PCTFE, we found good agreement of the rigid fraction with DSC estimates of crystallinity, when the sample was measured above Tg and using a spin lock frequency of 100 kHz. Given this previous success to access crystallinity with NMR, we applied these same techniques to FK-800.

A representative example of the SCORE processed $T_{1\rho}$ data for a FK-800 lot without impurities is given in Figure 8a. The spectral filter shows the mobile and rigid components are heavily overlapping and that a higher proportion of the -CF2- fluorines are mobile in comparison to the -CClF- fluorines. The $T_{1\rho}$ curve shows a bi-exponential behavior for the two components with the mobile phase having a $T_{1\rho}$ relaxation time close to 1 ms and the rigid having a longer relaxation time of 5.45 ms. All the lots without impurities can be adequately fit with two components, whereas lots with impurities require three components. Figure 8b shows the SCORE-processed $T_{1\rho}$ data for FK-800 lot C which has an impurity at -123 ppm. Notably this impurity has a significantly longer $T_{1\rho}$ relaxation time than the constituent phases however the impurity signal only contributes about 2% towards the total signal, implying a low concentration. The vastly different $T_{1\rho}$ relaxation time of the impurity indicates that the impurity is phase separated from the surrounding polymer matrix; otherwise spin diffusion effects would average out the measured $T_{1\rho}$ relaxation time. This observation of a distinct relaxation times can be used to estimate the length scale of the heterogeneity using the expression for the maximum spin diffusion path length, r:

$$\langle r \rangle = \sqrt{6D\tau} \qquad (2)$$

where D is the spin diffusion coefficient, assumed to have a value of 0.1 nm2/ms and τ is the relaxation time[4].Using the relaxation time for the impurity phase provides a maximum spin diffusion path length of ~4.4 nm, and suggests that the heterogeneity is larger than 4.4 nm. Spin diffusion also impacts a spin lattice relaxation (T1) measurement, which can provide an upper bound for heterogeneity size. Only one T1 value is obtained (2.4 s) indicating spin diffusion is averaging the inherent T1 relaxation times of each of the phases, otherwise multiple T1 values could be obtained if the samples were well separated by 100 nm length scales. Using the same equation with the T1 relaxation time gives an upper bound of the heterogeneity of ~38 nm for the impurity phase. The observation of an impurity in this lot is notable as this lot displays anomalous fast crystallization kinetics and indicates this impurity may be playing a role as a nucleating agent for crystallization. Thus far, AFM data does not show morphological evidence of large 4-38 nm sized particles within the film.

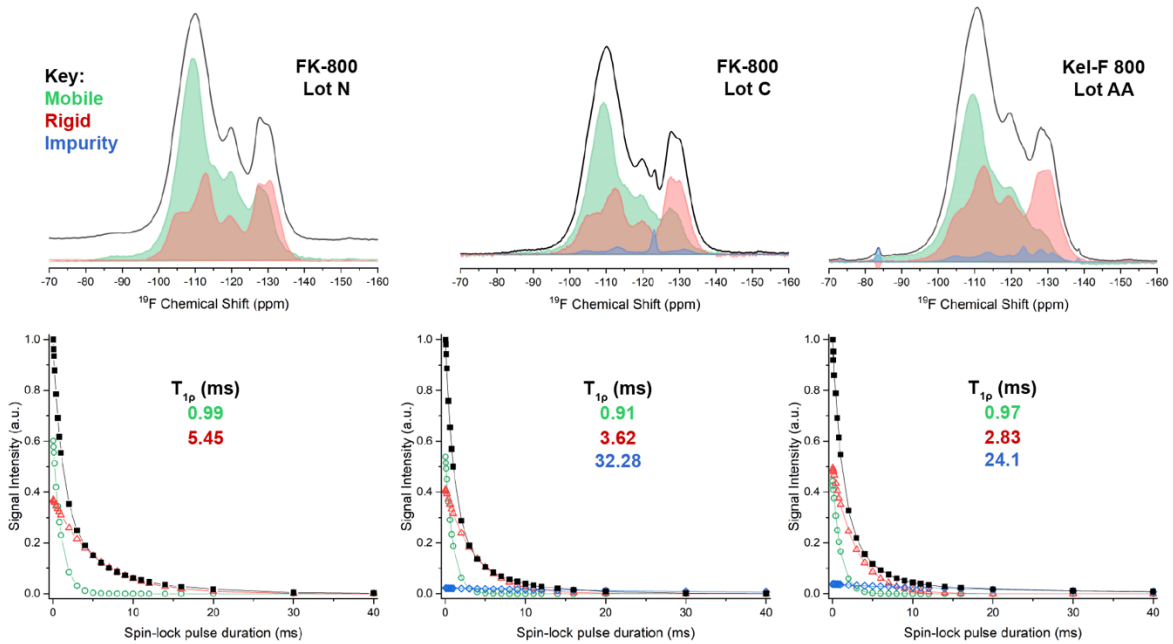

Figure 8 Solid-state ^{19}F NMR spectra (black) with $T_{1\rho}$ spectral filtered mobile (green), rigid (red), and impurity (blue) components with corresponding $T_{1\rho}$ decay below. (a) FK-800 lot N, collected at 50°C after an isothermal hold for 4192 minutes. (b) FK-800 lot C, collected at 50°C after a isothermal hold for 276 minutes. (c) of Kel-F 800 lot AA, collected at 25°C with an unknown thermal history.

The impurities observed in Kel-F 800 lots display behavior similar to the impurity in the FK-800 lot C impurity. They have much higher $T_{1\rho}$ relaxation times than the constituent rigid and mobile phases of the network polymer and imply these are heterogeneous impurities in the polymer rather than incorporated homogeneously into the polymer chain. As such, bounds to the impurity size can be determined by the $T_{1\rho}$ relaxation time and the T1 measurement, which also only has 1 relaxation time of 1.7s. This places the length scale of the heterogeneity between 3.8 to 32 nm. Additionally, the $T_{1\rho}$ filtered spectra reveals more information of the chemical environments of this impurity where it is more obvious there is peak at -123 ppm and implies the **impurities observed between the Kel-F 800 lots and the impurity observed in FK-800 lot C have similar chemical environments** and potentially from the same origin. The application of a $T_{1\rho}$ filter can provide further insights into the chemical identity when combined with ^{19}F-^{13}C correlation measurements.

Summary of NMR spectral features:

- As expected, Kel-F has more impurities than FK-800.
- Impurities are phase separated from the surrounding polymer matrix
- Sizes bounded by NMR response in range of 4-40nm
- Impurities observed in Kel-F 800 lots and the impurity observed in FK-800 lot C have similar chemical environments, possibly stemming from the same source

2.3 Multi-modal Characterization for lot N

In this section we detail progress on multi-modal studies that investigate the temperature dependence of crystallization. Last year we used hot-stage AFM of thin films (lot N) to demonstrate the glassy

behavior of FK-800. We showed that at high driving forces (closer to T_g) the samples had high nucleation densities but kinetically-slow radial growth rates resulting in rough film moprphologies like Figure 9b, whereas at low driving forces (closer to the melt temperature, T_m), samples had lower nucleation density and thermodynamically slow radial growth rates leading to a few islands with very smooth edges like the morphology shown in Figure 9e. In between these two extremes (near 50°C, red curve) , we found that overall fastest total growth rates with both high nucleation density and high radial growth rates (Figure 9a). This FY we have used this work as a foundation for time resolved DSC and NMR studies on bulk samples with the goal of (a) correlating and where possible calibrating crystallization signatures and (b) developing methods capable of measuring crystallization within bulk composites.

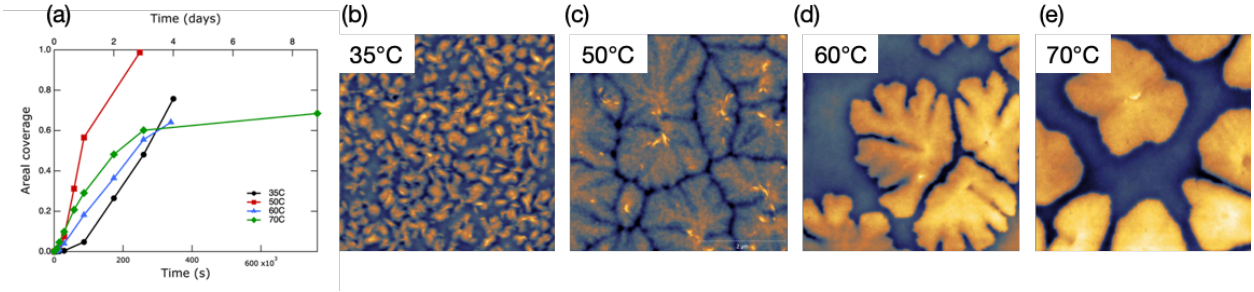

Figure 9. (a) Crystalline coverage of thin films aged at 35 (black), 50 (red), 60 (blue), and 70°C (green) as measured by hot-stage AFM. (b-e) corresponding images after ~3 days of thermal aging. The film aged at 50°C has the highest coverage. Images are 5µmx5µm. (b,c) have a z-scale of 20nm whereas (d,e) have a z-scale of 30nm.

2.3.1 Tracking crystallization using DSC

Figure 10 uses differential scanning calorimetry (DSC) to track the crystallinity evolution of Lot N films aged at different temperatures for ~40 days. All samples initially crystallized rapidly within 4 days, then stabilized as is highlighted by the peaked crystallization rate data (Figure 10b). By day 40, 50°C samples achieved the highest crystallinity (18.6%), followed closely by 60°C. The 70°C rate was slower than 60°C, and 35°C exhibited the slowest overall kinetics, reaching only 13.6% crystallinity.

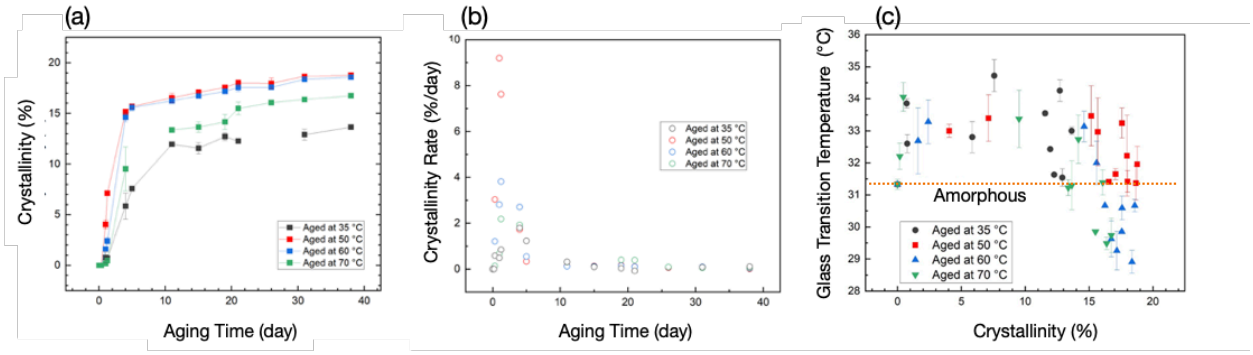

Figure 10. Relative crystallinity of Lot N films as a function of aging time under different aging temperatures. And the solid black line indicates the corresponding Avrami fitting.

Figure 10c reveals an interesting relationship between the glass transition temperature, T_g, and crystallinity in Lot N films. All samples start in the amorphous state with a T_g ~31.3°C. Despite the evident data noise, a non-intuitive trend emerges: T_g initially climbs with increasing crystallinity up to ~10%, likely due to restricted mobility in the amorphous phase near crystalline interfaces[5]. Beyond

~15% crystallinity, however, T_g surprisingly dips below the amorphous value, especially at higher crystallinities (>18%). This unexpected behavior, where the highly crystalline phase exhibits a lower T_g than the amorphous state, has been observed in other materials [5]. One potential explanation, as reported in the literature, is an abnormal density difference where the amorphous phase is denser than the crystalline phase [3]. However, further investigation is necessary to determine if this explanation applies to FK-800 and elucidate the underlying mechanism for this unexpected Tg decrease.

2.3.2 Tracking crystallization kinetics using in situ and ex situ NMR approaches

This FY we initiated in situ NMR to track crystallization during thermal aging to mirror hot-stage AFM and ex situ DSC experiments. The goals of this study were to: (a) calibrate multimodal analysis and (b) shed light on the timescales and molecular moieties associated with the transformation from amorphous to crystalline phases.

Figure 11 shows an example spectrum from a lot N sample, obtained during an in-situ isothermal experiment at 50°C for 3.5 days. After 3.5 days of crystallization (red line), the spectrum exhibits subtle changes compared to the initial amorphous state (purple line). Broadening is observed in the -CF2- and -CClF- regions (associated with CTFE), indicating its crystallization, while the VDF region remains unchanged. Based on DSC results on parallel aged samples (described above), the crystallinity after this duration is expected to be around ~15%. The lack of obvious changes to the spectra with crystallization speaks to the extreme broadening from not only structural disorder but also strong heteronuclear and homonuclear interactions and ^{19}F chemical shift anisotropy. These factors can mask the signals of crystalline domains within the spectrum highlighting the need for advanced filtering techniques like the $T_{1\rho}$ filter to effectively separate and analyze the crystalline (rigid) and amorphous (mobile) phases.

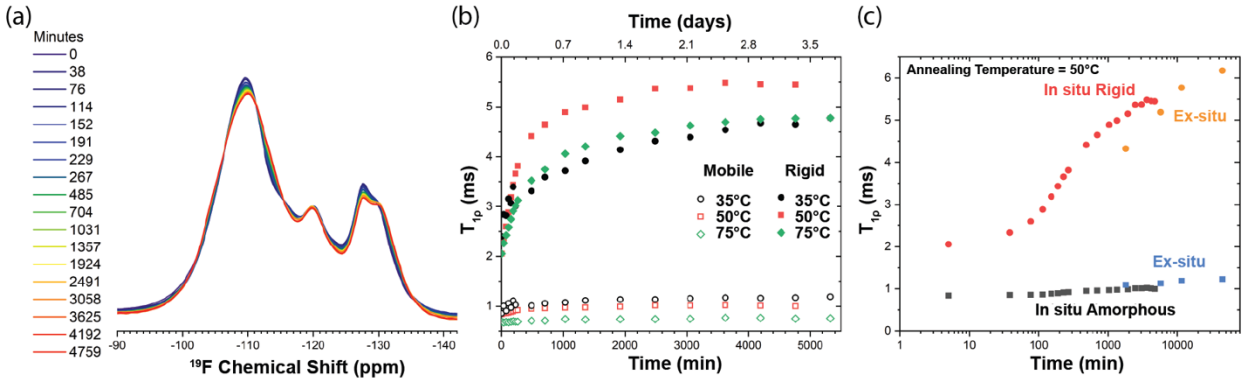

Figure 11 (a) Solid-state ^{19}F NMR spectra of FK-800 lot N held at 50°C and recorded at the durations provided in the legend. The subtle changes in the line shape are due to crystallization(b) $T_{1\rho}$ values of mobile and rigid components from in situ isothermal $T_{1\rho}$ experiments at 35, 50, and 70°C. (c) Comparison of the in situ $T_{1\rho}$ values at 50°C to $T_{1\rho}$ values obtained on samples aged ex situ.

Application of $T_{1\rho}$ measurements and SCORE processing like that shown in Figure 8, produce a $T_{1\rho}$ filtered component spectra, its associated $T_{1\rho}$ relaxation time, and their signal fraction. The $T_{1\rho}$ relaxation times for the mobile and rigid components from these in situ crystallization experiments are shown in Figure 11 for three temperatures 35°C, 50°C, and 75°C. The relaxation time, $T_{1\rho}$, of the amorphous mobile component does not change much with aging time; this might be expected because the molecular motions of most of the amorphous phase don't change significantly when the crystallization is low

(<15%). On the other hand, the rigid components change dramatically with aging time, where for each temperature there is a rapid increase in the $T_{1\rho}$ within the first few hours of crystallization followed by a slower process. Qualitatively this behavior resembles that of crystallization growth rates as measured by AFM and DSC. The increase in the $T_{1\rho}$ values with crystallization reflects the growing crystalline domains in the sample. It is interesting to note the $T_{1\rho}$ values of at 50°C are higher than those at 35°C or 70°Cas also seen by AFM (Figure 9a). This indicates that the $T_{1\rho}$ value of the rigid component may serve as a qualitative measure of the degree of crystallization in FK-800.

To validate the changes observed in the in situ measurements, parallel samples were aged in an oven at 50°C and then DSC was collected to determine the percent crystallinity. $T_{1\rho}$ values were obtained on these samples for comparison (Figure 9). The ex situ and in situ aged mobile component are in reasonable agreement. (The slight discrepancy may be due to the centrifugual forces on the spinning in situ sample that could affect crystallization kinetics.)

Summary of NMR in situ studies:

- Crystallization causes subtle changes to the spectral line shape - broadening in the -CF2- and -CClF- regions.
- Spectral filtering of $T_{1\rho}$ shows qualitative trends with crystallization; namely the time constant of the rigid fraction of $T_{1\rho}$ increases with thermal treatments/crystallization, qualitatively reproducing expected temperature trends at 35°C, 50°C and 70°C

2.3.3 Correlating NMR metrics with DSC

We investigated two strategies to quantitatively relate NMR metrics with percent crystallinity (using measured by DSC): the rigid fraction of T1ρ and spectral differences before and after aging.

As the SCORE processing of T1ρ provides a fraction of each component, in theory the rigid fraction should reflect the overall bulk crystallinity. Previously we saw good agreement of these two in PCTFE, however in FK-800 the results are not in good agreement, as detailed in Figure 12. At all temperatures we expect the crystallinity to start near zero and increase with time as is seen by DSC (Figure 12a) and is suggested by the increasing T1ρ time constant (Figure 12bd). Instead the rigid fraction collected at 35°C (black) has high scatter with a starting value near ~0.5 and displays a slight decrease with aging time. The in situ rigid fractions for 50°C (red) and 70°C (green) show an expected increase at early aging times but the values themselves start at ~0.35 rather than zero as would be expected for a purely amorphous sample at time zero. Similarly, ex situ rigid fraction values for mirror samples with corresponding DSC data remained consistently around 0.35 (red open squares), contrasting with DSC measurements that showed a gradual increase from zero to approximately 0.15 (open blue diamonds).

These results suggest the application of $T_{1\rho}$ to obtain bulk crystallinity estimates in FK-800 is not accurate. A possible explanation is from the experimental conditions used in the T1ρ measurement, where in the measurement probes motions at a specific frequency set by the RF spin lock frequency. For all $T_{1\rho}$ measurements the spin lock frequency has been kept at 100 kHz. Dielectric spectroscopy measurements probe the same motional frequency range as T1ρ measurements, and in previous detailed studies in literature on PCTFE a γ relaxation mode present in both crystalline and amorphous phases is centered at 100 kHz when above Tg[7-9]. This correspondence indicates the T1ρ measurements were able to accurate predict crystallinity in PCTFE because they were measuring the γ relaxation motions that were evenly present in both phases. The addition of PVDF to PCTFE for FK-800

very likely changed the motional frequency range of the γ relaxation, thus the current T1ρ experimental conditions are not measuring the correct ratio of the crystalline and amorphous components to the γ relaxation. We are currently conducting dielectric measurements to determine frequency and temperature of the γ relaxation peak maximum. Ideally this information will enable us to calibrate the $T_{1\rho}$ spin lock frequency for a specific temperature regime to be able to produce accurate estimates of crystallinity.

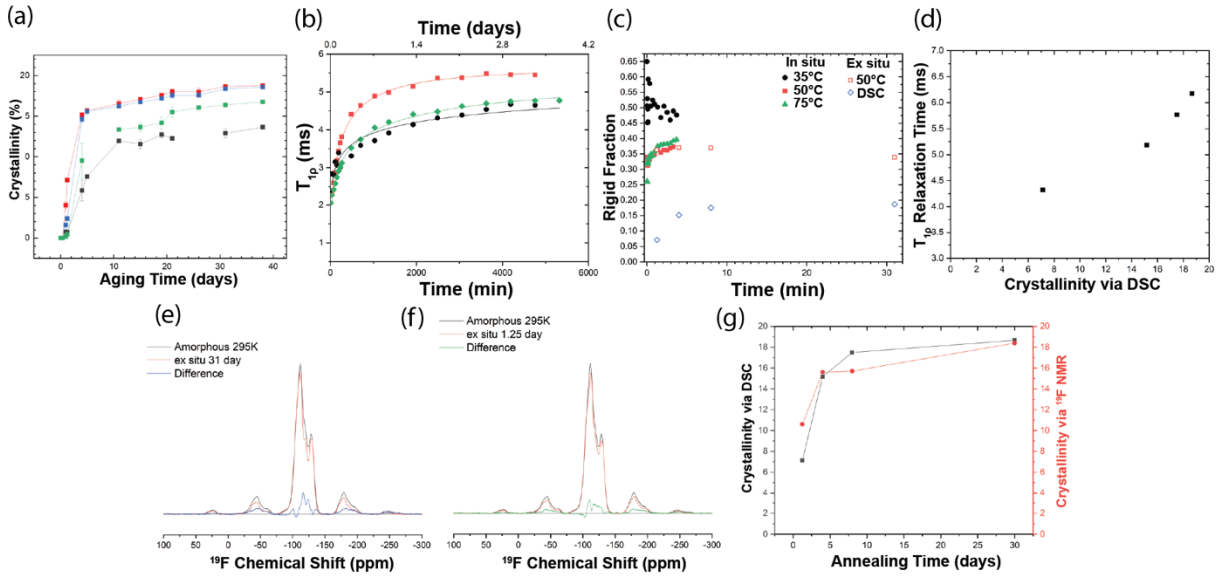

Figure 12. DSC and NMR signatures of FK-800 crystallization as a function time and temperature for Lot N at 35°C (black), 50°C (red), 60°C (blue) and 70°C (green). (a) % crystallinity determined from DSC. (b) Relaxation time for the rigid (crystalline) component of spectrally filtered $T_{1\rho}$ measurements from ^{19}F NMR (c) The fraction of the rigid component to the $T_{1\rho}$ signal from in situ isothermal measurements and ex situ aged samples. The crystalline fraction as measured by DSC is plotted for comparison. (d) The correlation between T1rho and percent crystallinity (as measured by DSC). (e,f) Two exemplary spectra comparing the starting amorphous phase (black), thermally aged samples (red) and the difference (green). (g) Percent crystallinity verus time for samples aged at 50°C as measure by DSC (black) and spectral difference (red).

As a second strategy to quantify crystallinity, we re-investigated spectral differences during aging. Two exemplary spectra at early and late aging times are shown in Figure 12ef with the starting amorphous stage in black, crystallized sample in red, and the difference in green. By integrating the area under the difference spectra and comparing it with the area under the starting amorphous curve, we can extract a percent crystallinity. Figure 12g shows that the % crystallinity of the ex situ samples aged at 50°C (black) the % crystallinity from the difference spectrum (red) are in reasonable agreement. In FY24 we will test this scheme for a broader range of conditions.

Summary of multi-modal signatures of crystallization:

- DSC shows expected trends in the time-scale and % crystallinity, in qualitative agreement with those found via AFM.
- In contrast to PCTFE, FK-800 has poor quantitative agreement between rigid fraction of T1rho and the degree of crystallization. We plan to use impedance spectroscopy to determine whether we are measuring in an appropriate frequency window.
- Percent crystallinity determined from integrating spectral differences shows good quantitative agreement with DSC.

3 Project Summary and Outlook

The objective of this task is to utilize advanced methods to quantitatively assess changes in fluoropolymers due to aging stressors. We focused on using hot-stage AFM data to generate crystallization metrics for all lots that will be part of a crystallization database. As shown in this report, we have extracted fundamental crystallization metrics for both FK-800 and Kel-F lots.

In addition, we incorporated NMR to better correlate multi-modal analysis of crystallization. The project will ascertain the degree to which NMR can provide a quantitative measure of the degree of crystallization.

This year we showed:

- Current lots vary in their crystallization parameters with the nucleation density ranging from 0.05 and 13.5 μm^{-2}, two orders of magnitude and growth rates that vary from from 8 x 10^{-13} to 1 x10^{-11} m/s one order of magnitude.
- The nucleation density and growth rate were not always correlated suggesting effects other than supersaturation.
- Lots can be categorized based on whether their nucleation and their growth rate. Alternatively, these groupings can be obtained from the Avrami exponent and rate constants.

In future work we hope to complete our survey of current lots and to develop categorization schemes that will help predict which lots are expected to have similar aging behaviors. The analysis of the AFM data in this report was performed by hand which is very time-consuming. We have efforts to speed and improve this process using machine learning tools in collaboration with Case Western Reserve University (CWRU). The expectation is that these tools will improve accuracy and detect correlations that we have not uncovered.

By combining imaging, diffraction, scattering, calorimetry and NMR we are developing a more complete picture of aging processes in aged fluoropolymers. This data will be used to determine whether crystallization signatures such as nucleation density, crystallization rate, Avrami constants, and Avrami exponents can be linked to processing or aging behavior. For example, the crystallization behavior is likely to be correlated with wetting, adhesion and mechanical strength.

4 References

1 Lu, M., Venkat, S., Augustino, J., Meshnick, D., Jimenez, J., Tripathi, P., Orme, C. A., Wu, Y., Bruckman, L. S., French, R. H., “Image Processing Pipeline for Fluoroelastomer Crystallite Detection in Atomic Force Microscopy Images (U)” Integr Mater Manuf Innov 12, 371–385 (2023). https://doi.org/10.1007/s40192-023-00320-8 (U Document), (LLNL-JRNL-853058)

2 Tatsuno, H.; Aimi, K.; Ando, S. Solid-State 19F MAS NMR Study on the Conformation and Molecular Mobility of Poly(Chlorotrifluoroethylene). Magn. Reson. Chem. 2007, 45 (5), 401–409. https://doi.org/10.1002/mrc.1982.

3 Nilsson, M.; Morris, G. A. Speedy Component Resolution: An Improved Tool for Processing Diffusion-Ordered Spectroscopy Data. Anal. Chem. 2008, 80 (10), 3777–3782. https://doi.org/10.1021/ac7025833.

4 McBrierty, V. Solid Polymers: A Challenge for NMR. Solid State Nuclear Magnetic Resonance 1997, 9 (1), 21–27. https://doi.org/10.1016/S0926-2040(97)00039-8.

5 Struik, L. C. E. The mechanical and physical ageing of semicrystalline polymers: 1 Polymer 1987, 28, 1521.

6 Rånby, B. G., Chan, K. S., and Brumberger, H. Higher-order transitions in poly(4-methyl-1-pentene) Journal of Polymer Science 1962, 58, 545.

7 Hoffman, J. D.; Williams, G.; Passaglia, E. Analysis of the α, β, and γ Relaxations in Polychlorotrifluoroethylene and Polyethylene: Dielectric and Mechanical Properties. J. polym. sci., C Polym. symp. 1966, 14 (1), 173–235. https://doi.org/10.1002/polc.5070140116.

8 Samara, G. A.; Fritz, I. J. Pressure and Temperature Dependence of the Dielectric and Ultrasonic Properties of Polychlorotrifluoroethylene (PCTFE). J. Polym. Sci. B Polym. Lett. Ed. 1975, 13 (2), 93–99. https://doi.org/10.1002/pol.1975.130130207.

9 Sacher, E. Dielectric Demonstration of Crystalline and Amorphous Peaks in PCTFE. J. Polym. Sci. B Polym. Lett. Ed. 1980, 18 (5), 333–337. https://doi.org/10.1002/pol.1980.130180503.